Biochemistry

 Volume 37, Number 26 June 30, 1998

Articles

Understanding the Role of the Essential Asp251 in Cytochrome P450cam Using Site-Directed Mutagenesis, Crystallography, and Kinetic Solvent Isotope Effect†

Momcilo Vidakovic,‡ Stephen G. Sligar,*,‡ Huiying Li,§ and Thomas L. Poulos*,§

Department of Biochemistry and the Beckman Institute for Advanced Science and Technology, University of Illinois at Urbana−Champaign, Urbana, Illinois 61801, and Department of Molecular Biology and Biochemistry, University of California at Irvine, Irvine, California 92697

Received January 26, 1998; Revised Manuscript Received April 23, 1998

ABSTRACT: Proton transfer in cytochromes P450 is a critical step in the activation of molecular oxygen. Extensive study of the P450cam active site has identified several residues that play a central role in dioxygen bond scission. A highly conserved carboxylate, aspartate-251 in P450cam in the distal helix I, participates in a series of hydrogen-bond/ion pairs near the molecular surface and has been implicated in the catalytic mechanism. Mutation of Asp251 is known to lower activity by 2 orders of magnitude and change the rate-limiting step in the catalytic cycle, suggesting a role for an acid functionality in generation of iron−oxygen reactive intermediates. The turnover rates of the Asp251Asn mutant in various protium-deuterium mixtures have been determined and show a significantly larger kinetic solvent isotope effect, with an overall magnitude of 10 compared to 1.8 for the wild-type P450cam. In addition, a much larger number of protons are involved in the rate-limiting step for the Asp251Asn mutant than in the wild-type enzyme. These results indicate that Asp251 is an essential part of the normal proton delivery machinery required for O−O bond scission. The crystal structure of the Aps251Asn mutant obtained from data collected at cryogenic temperatures has been refined to 1.9 Å. Key hydrogen bonds required to hold Asp251 in position have been broken which allows the mutant Asn251 side chain to swing out and away from the O_2 binding site leading to a more open active site. This change could allow easier access by water and thus contribute to the observed kinetic solvent isotope effects.

Cytochromes P450 are heme containing monooxygenases found throughout the biosphere that catalyze the monooxygenation of a wide variety of hydrophobic substrates. Much of the detailed P450 structure−function work has focused on the bacterial P450cam, primarily because this was the first soluble P450 to be purified in large quantities (*1*) and have its sequence (*2*, *3*) and X-ray structure determined (*4*). Many of the studies on P450cam have focused on elucidating the structural and mechanistic details of the catalytic cycle outlined in Figure 1. The intermediates **1**−**3** have been characterized, including determination of the crystal structures for **1** and **2** for both P450cam (*4*, *5*) and P450BM3 (*6*−*8*). The ferrous (Fe^{2+})−carbon monoxy complex of P450cam has served as a model for the oxy intermediate **3** (*9*). The existence of the remaining intermediates has only been inferred, and the structure of these hypothetical species is based on what is known from other heme enzyme systems.

† This work is supported by National Institutes of Health Grants GM32688 (T.L.P.), GM31756 (S.G.S.), and GM33775 (S.G.S.).

* Authors to whom correspondence should be addressed. E-mail: poulos@uci.edu. Phone: (714) 824-7020. Fax: (714) 824-3280. E-mail: sligar@uiuc.edu. Phone: (217) 244-7395. Fax: (217) 244-7100.

‡ University of Illinois.

§ University of California.

S0006-2960(98)00189-5 CCC: $15.00
Published on Web 06/11/1998

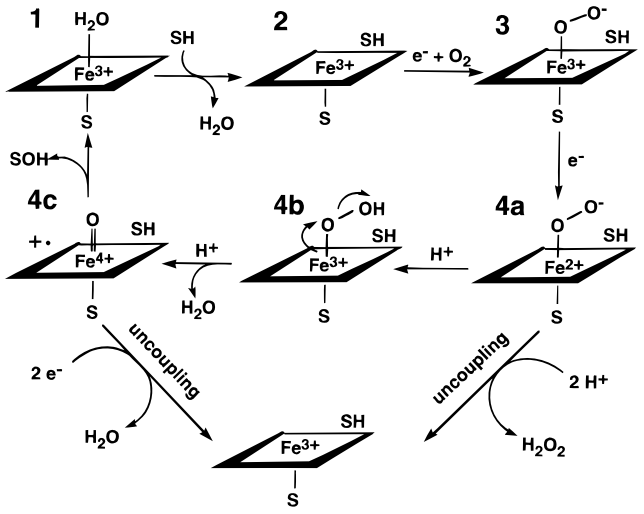

FIGURE 1: Schematic diagram of the P450cam catalytic cycle. SH represents the substrate, camphor.

For example, the active oxygenating species, **4c** (Figure 1), shown as an oxy−ferryl center with an organic cation radical, is analogous to the well-known peroxidase compound I intermediate. Nevertheless, it is not known if this is the true electronic structure of **4c**.

Various attempts have been made to identify the expected intermediates shown in Figure 1 ranging from site-directed mutagenesis to the use of various analogues of the natural substrate, camphor, to alter the rate-limiting step of the reaction (*10*). However, manipulation of the P450 system, especially by mutagenesis, often leads to uncoupling (Figure 1) where reducing equivalents derived from reduced pyridine nucleotides are shuttled into the unproductive formation of water and/or peroxide. For example, the conserved residue Thr252 that forms part of the O_2 binding site has been postulated to play a key role in a proton delivery system to the iron-linked dioxygen which is required for cleavage of the O−O bond (Figure 1). Converting Thr252 to other residues results in uncoupling (*11*−*13*), which makes it difficult to assess the role that Thr252 plays in the productive pathway leading to hydroxylated product. This has proven to be long-standing general problem in attempts to identify transient intermediates in the P450 reaction cycle.

A mutant or set of mutants that changes the rate-limiting step in the reaction cycle without leading to uncoupling is a highly desirable goal. In this way, short-lived intermediates will build up, allowing their identification by various biophysical probes. Shimada et al. (*14*) and Gerber and Sligar (*15, 16*) have identified a mutant with these properties. Conversion of Asp251 to Asn lowers the overall rate by 2 orders of magnitude with little uncoupling (*16, 17*). Most importantly, a new spectral intermediate builds up under steady-state conditions with a visible absorption spectrum that clearly does not resemble the ferrous−oxy complex. Benson et al. (*17*) suggested that this intermediate is most likely **4a** in Figure 1 and that protonation of **4a** is rate limiting in the mutant. These results have lead to the proposal that conversion of Asp251 to Asn disrupts the proton delivery machinery required for cleaving the O−O bond. Recent studies of the oxygen activation process in the wild-type P450cam using a kinetic solvent isotope effect (KSIE) approach (*18*) revealed the second electron transfer as the only step in the catalytic cycle to display a discernible KSIE with a magnitude of 1.8. On the basis of this evidence, it was proposed that a proton transfer event, which is partially rate limiting in the wild-type P450cam, facilitated dioxygen bond cleavage and formation of a high-valent iron−oxo intermediate (**4c**). Extensive mutagenesis studies (*11, 12, 14*−*16*) suggested that Asp251 and Thr252 serve as a proton delivery conduit involving the participation of solvent water which leads to oxygen activation. To shed more light on the mechanism of proton transfer in cytochrome P450cam, we have applied the KSIE methodology to mutation at the acidic active site residue implicated in the proton delivery event along with the analysis of 1.75 Å wild-type and 1.9 Å Asp251Asn mutant crystal structures obtained from X-ray intensity data collected at cryogenic temperatures.

EXPERIMENTAL SECTION

Enzyme Assays. Wild-type and mutant P450cam, putidaredoxin, and putidaredoxin reductase were expressed in *E. coli* and purified using published procedures (*16*). All kinetic assays were performed under V_{max} conditions. A typical NADH oxidation reaction consisted of a reconstituted systems with 1μM P450cam, 12μM putidaredoxin, 2.2μM putidaredoxin reductase, and 500μM 1R-(+)-camphor in 50mM phosphate buffer at the appropriate pH. Oxidation of NADH was followed at 340 nm using an extinction coefficient of 6.22 mM^{-1} cm^{-1}. Product was analyzed using gas chromatography. Reaction volumes of 400 μL consisting of the reconstituted system were quenched at various time points with 2M potassium hydroxide. Upon addition of *endo*-3-bromocamphor, which served as an internal standard, reaction mixtures were extracted with three volumes of chloroform and dried with magnesium sulfate under a stream of dry nitrogen. Gas chromatographic analysis was carried out using a cross-linked 5% methyl phenyl siloxane column with a single ramp temperature program (*17*). Signals with retention times of 7.8, 11.4, and 12.3 min corresponding to 1R-(+)-camphor, *exo*-5-hydroxycamphor, and *endo*-5-bromocamphor, respectively, were integrated and used to define product concentration. Previous work had shown that the flame ionization of the internal standard and *exo*-5-hydroxycamphor are identical.

Kinetic Solvent Isotope Methods. Buffer solutions were prepared by lyophilizing potassium phosphate buffers and then dissolving the dry residue in D_2O. Stock solutions of the proteins were equilibrated prior to each experiment in the freshly prepared H_2O/D_2O buffer mixtures before measuring enzyme activities. The pL of the buffer was determined using the equation $pL = pH_{obs} + 0.311x + 0.0766x^2$ where x represents the fraction of deuterium in solution (*19*).

Catalytic turnover rate constants and product formation rates were analyzed using a nonlinear regression analysis. Experimental points from the product formation rates in various isotopic mixtures were fitted to the following equation:

$$k_x/k_H = \Pi(1 - x + x\phi_i)^{TS}/\Pi(1 - x + x\phi_j)^{RS} \quad (1)$$

where x is the atomic fraction of deuterium used in the experiment, and ϕ_i and ϕ_j are the isotopic fractionation factors and represent the respective fraction of deuterium bound at sites i and j relative to the fraction of deuterium present in bulk solvent. ϕ is thus a measure of the relative affinity of

Table 1: Summary of Data Collection Statistics and Crystallographic Refinement

	wild-type	Asp251Asn mutant
data collection system	Siemens ×1000 2 crystals	SSRL[a] beam line 7-1 1 crystal
cell dimensions(Å)	$a = 106.3$	$a = 106.6$
	$b = 103.3$	$b = 103.2$
	$c = 36.5$	$c = 36.6$
total observations	179 587	98 277
unique reflections	37 112	31 326
R_{sym}[b]	0.058	0.049
% completeness total	89.7	96.0
% completeness	97.9 (2.1−1.9 Å)	
highest resolution shell	54.7 (1.9−1.75 Å)	96.6 (1.93−1.90 Å)
$I/s(I)$ in highest resolution shell	1.6	5.8
reflections used for refinment $F>2s(F)$	32 995 (10.0−1.75 Å)	29 283 (10.0−1.9 Å)
R[c] factor	0.21	0.20
R_{free}	0.26	0.27
RMS[d] deviation bonds (Å)	0.009	0.009
RMS deviation angles (degrees)	1.5	1.5

[a] SSRL, Stanford Synchrotron Radiation Lab. [b] $R_{sym} = S|I_i - \langle I_i \rangle| / SI_i$, where Ii is the intensity of the ith observation and $\langle I_i \rangle$ is the mean intensity. [c] $R = \sum|F_o - F_c|/\sum|F_o|$; R_{free} = free R factor based on 5% of the reflections. [d] The RMS deviations of bond parameters represent the root-mean-square deviations from ideal values.

the site for deuterium. k_x and k_H are the measured rates in D_2O/H_2O mixtures and H_2O alone, respectively, and TS and RS refer to the transition state and reactants, respectively. The goodness of fit and the number of protons in flight in the transition state were analyzed by an iterative multicomponent least-squares process.

Crystallography. Crystals were grown according to the established capillary free interface method (*20*). The mutant crystals rapidly decayed under the X-ray exposure at room temperature. Therefore, cryogenic data were collected using 20% glycerol plus 10% sucrose as cryoprotectants. Crystals were transferred stepwise to the artificial mother liquor (40% saturated ammonium sulfate, 250 mM KCl, 200 μM camphor, 50 mM KPi, pH 7.0) containing increasing amounts of cryoprotectants (5% increment) before being flash frozen in a cold stream of nitrogen gas at 100 K. The Asp251Asn mutant data set was collected at the Stanford Synchrotron Radiation Facility (SSRL) beamline 7-1, which is equipped with a Mar imaging plate and a monochromatic X-ray source at 1.08 Å. The wild-type cryogenic data were collected using a Siemens X-1000 area detector with a copper rotating anode and Supper double mirror focusing optics.

The wild-type data were processed with XDS (*21*), and then reflection intensities were converted to structure factor amplitude format for XPLOR (*22*) through CCP4 (*23*). The Asp251Asn mutant data were reduced using DENZO and SCALEPACK (*24*), and again CCP4 to generate structure factors. The subsequent model building and refinement cycles were carried out on a Silicon Graphics Indigo workstation using TOM/FRODO (*25*) and X-PLOR, respectively. Due to the unit cell shrinkage in the cryogenic data, the room-temperature P450cam model had to be repositioned by running molecular replacement with AMoRe (*26*). Additional water molecules in the cryogenic data were added by hand based on Fo-Fc density maps contoured at 3.0σ. Free R factors were monitored during the water picking to avoid overfitting. The statistics of data collection and refinement for both data sets are summarized in Table 1. The atomic coordinates of both structures have been deposited with Brookhaven Protein Data Bank (filenames 5CP4, 6CP4).

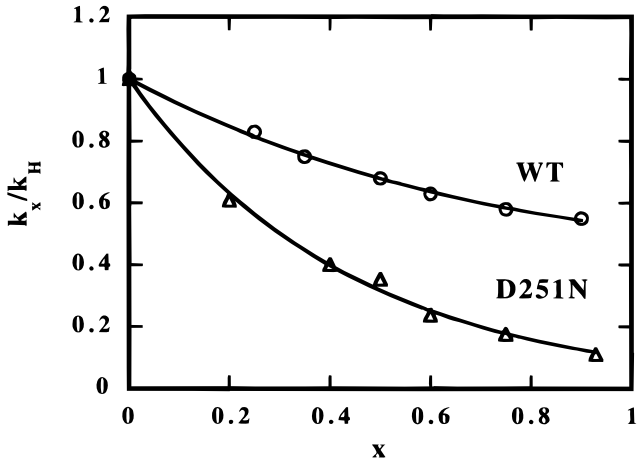

FIGURE 2: Proton inventory for wild-type P450cam and the Asp251Asn mutant. The fraction of deuterium (x) is plotted against the ratio of steady-state activity measured in the H_2O/D_2O mixture (k_x) to the rate measure in H_2O (k_H). The solid lines represent the best fit of the experimental data to eq 1. Standard measurement errors are given in Table 2.

RESULTS

Kinetic Solvent Isotope Effects. The overall rate-limiting step in the P450cam catalytic cycle is the second electron-transfer step, **3** to **4** (Figure 1) (*27*). Since spectral intermediates characteristic of **4b** and **4c** in Figure 1 have not been observed in a fully reconstituted P450cam system, then the various steps between **4a** back to the resting state (**1** in Figure 1) are not limiting. The only step in the P450cam cycle to display a significant KSIE is the second electron-transfer step, **3** to **4** in Figure 1 (*18*). The KSIE = 1.8 for this step shows that proton transfer is involved in the relatively slow second electron-transfer step. Since the Asp251Asn mutant shows a build-up of a new intermediate thought to be **4a** in Figure 1 (*17*), it was reasoned that the new rate-limiting step in the mutant might be the transfer of a proton to **4a** to give **4b**. To explore this possibility, KSIE experiments were carried out and are summarized in Figure 2 and Table 2. The effect of deuterium on the NADH oxidation kinetics in the P450cam reconstituted system was investigated in mixed isotopic waters. The catalytic turnover of substrate was initiated by addition of NADH to the

Table 2: Summary of NADH Oxidation, Product Formation Rates, and KSIE[a] for the Wild-Type and Asp251Asn Cytochrome P-450cam

	NADH oxidation kinetics		product formation rates	
P-450cam	(nmol min^{-1} $nmol^{-1}$ heme)	KSIE	(nmol min^{-1} $nmol^{-1}$ heme)	KSIE
wild-type[b]	809	1.5 ± 0.15 (1.8 ± 0.05)[c]	820	1.7 ± 0.15
Asp251Asn[d]	22[e]	5.9 ± 0.2	26	10 ± 0.2

[a] The pH dependence of isotope effects follows the trend of pH dependence on the steady-state rates for NADH oxidation in the wild-type and Asp251Asn reconstituted system (*16*). [b] 50mM potassium buffer, pH 7.0. [c] Single-turnover experiments (*18*). [d] 50 mM potassium buffer, pH 5.9. Kinetic assays and KSIE experiments were performed at different pH values due to the following: (i) The only reasonable rates of NADH kinetics/product formation catalyzed by the Asp251Asn mutant are obtained at low pH values (e.g., at pH 7 the rate of NADH oxidation catalyzed by Asp251Asn is over 2 orders of magnitude slower relative to that of wild-type); (ii) Actual coupling is ≈100% at pH 7 and pH 5.9 for wild-type and Asp251Asn mutant, respectively. [e] Rates were corrected for background NADH oxidation.

reconstituted system in the presence of excess camphor, and the progress of the reaction was monitored by UV−vis spectrophotometry as a change in the absorbance at 340 nm corresponding to the oxidation of the reduced form of NADH. Separate experiments were made at increasing content of deuterium oxide in the solvent using precisely the same enzyme stock solutions throughout. Although a decrease in the NADH oxidation rate was observed for both wild-type and Asp251Asn in the presence of deuterated solvent, the magnitude of the overall effect was significantly different for these two proteins. The Asp251Asn mutant exhibits a much larger KSIE for NADH oxidation (5.9) relative to that for the wild-type protein (Table 2). Notably, the rates of *exo*-5-hydroxycamphor formation for the Asp251Asn reconstituted system in protium oxide are much slower relative to those for the wild-type protein. The overall KSIE of 10 at pL = 5.9 obtained from corresponding product formation rate assays in various protium-deuterium mixtures is significantly larger than that observed by monitoring the rates of NADH oxidation under the same conditions. This suggests that the rate-limiting step or steps for NADH oxidation kinetics are partially masked.

Proton Inventory Analysis. The catalytic rates for product formation for both wild-type and the Asp251Asn mutant are a strong function of solvent deuterium content and exhibit isotope effects of 1.8 and 10 for the wild-type and Asp251Asn reconstituted systems, respectively. The solid lines in Figure 2 represent the best fit obtained through nonlinear regression analysis of experimentally measured catalytic rates at increasing atomic fraction of deuterium. A dramatic increase in the magnitude of the KSIE is observed for the Asp251Asn mutant reconstituted system and suggests that proton transfer becomes the rate-limiting process in the catalytic cycle. This is consistent with the suggestion of Benson et al. (*17*) that a key intermediate, potentially a peroxo−iron complex, is observable in the Asp251Asn mutant of P450cam. The characteristic bowl-shaped curvatures of the experimental data points suggest that the conversion from the initial (reactant) state to the transition state involves multiple proton transfer (*28*). Proton inventory and nonlinear regression analysis of the experimental KSIE data with a mathematical model (eq 1) provides the opportunity for quantitative evaluation of proton transfer during oxygen activation. Figure 3 shows a contour plot of the sum of squared residuals obtained from the analysis of the KSIE data for the wild-type and Asp251Asn mutant proteins assuming $\phi^{RS} = 1$. There is clearly a large difference in the proton coupling for these two proteins in the rate-limiting step observed in these environments. This analysis indicates that the number of protons participating in the rate-limiting step of the mutant

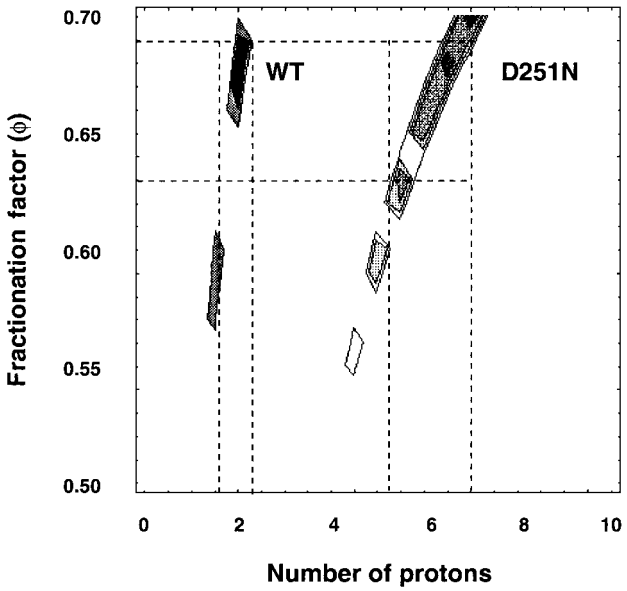

FIGURE 3: Fractionation factor description of KSIE data. The solvent isotope effect data for wild-type P450cam and the Asp251Asn mutant are analyzed according to the Schowen equation (*29*) assuming the reactant state contribution of one. The sum of squared residuals is presented as contours in a two-parameter fit using the intrinsic fractionation factor and the number of protons "in flight" in the quantitated transition state. The dotted lines indicate the number of protons assuming an expected range of fractionation factors between 0.63 and 0.69. Dark shaded areas correspond to the parameter space with the squared residuals of 0.0047 and 0.0031 for wild-type and the Asp251Asn protein, respectively.

protein is far larger than the corresponding number participating in the wild-type protein. For a range of expected fractionation factors (*28, 29*) the minimum number of protons involved in the transition state appears to be five. It has been postulated that at least two protons in flight in the transition state of the reaction lead to oxygen bond activation in the wild-type P450cam (*18*). The results of this study provide evidence supporting the proposed charge relay model (*15*) which involves a proton transfer from Asp251, when positioned in a favorable rotamer conformation, to the distal oxygen of twice reduced dioxygen complex through participation of bound water (*30*). In the transition state, this complex is believed to be stabilized by hydrogen bonding to residue Thr252 through an intervening water molecule (*4, 11*−*13*). In the absence of a polar side chain, Thr252 mutants exhibit loss of catalytic activity (*11, 12*) with the 10-fold increase in autoxidation rate (*12*).

pH Effects. A large change in catalytic activity with proton concentration has been reported for the wild-type protein and a number of mutants (*16*). While the activity of the

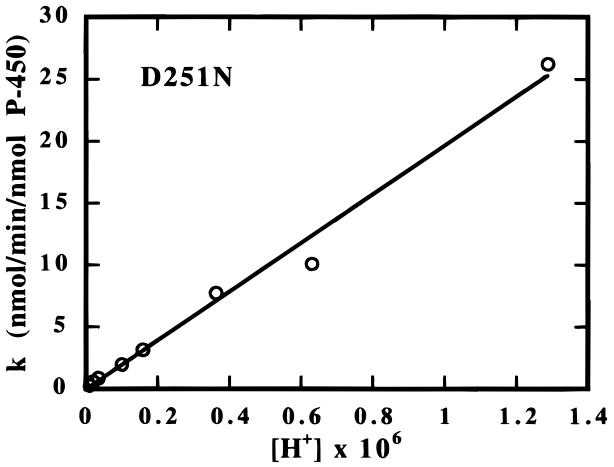

FIGURE 4: Effect of $[H^+]$ on product formation in the Asp251Asn mutant. Standard error limits are within the space of the symbols.

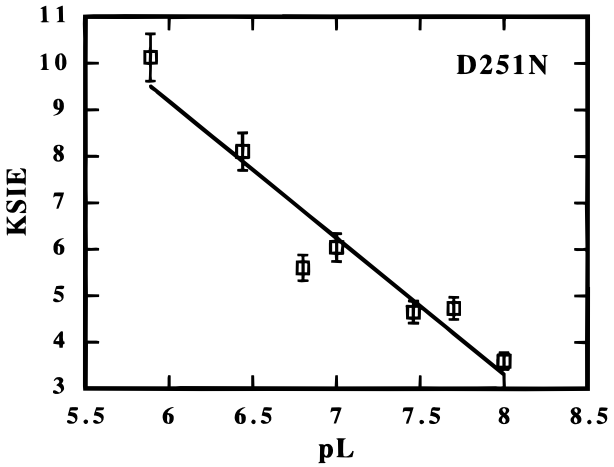

FIGURE 5: Effect of pL on the kinetic solvent isotope effect in the Asp251Asn reconstituted system.

Asp251Asn mutant at high pH is almost indistinguishable from the background level of putidaredoxin reductase and putidaredoxin autoxidation, and over 2 orders of magnitude slower than the wild-type, a significant portion of activity (roughly an order of magnitude) is recovered by decreasing the pH from 8 to 5. One interpretation offered by Gerber and Sligar is that the carboxylate side chain of Asp251 provides important catalytic (chemical) functionality for efficient proton transfer which is necessary for dioxygen bond scission. From the results reported here, mutation of Asp251 to Asn, a nonionizable side chain, abolishes this proton donating capabilities and forces the protein to utilize an alternative proton source. Since the rates of the substrate turnover linearly scale with the proton concentration (Figure 4), the alternative source of protons could be provided by internal solvent molecules communicating with the bulk water. Figure 5 shows the pL profile of the KSIE we observe for the Asp251Asn mutant of P450cam. Interestingly, the magnitude of the solvent isotope effect decreases with increasing pL. A potential explanation is that at higher pH (pL) values the concentration of the "proton transfer viable" species (i.e., H_2O/H_3O^+) is depleted and therefore fewer sites become available within a proton-transfer pathway that is critical for dioxygen activation. This would then result in a smaller observed KSIE.

Wild-Type Structures at Cryogenic Temperatures. The Asp251Asn mutant crystal structure was determined to see whether the hydrogen-bonding pattern thought to be required for the proton delivery mechanism has been disrupted. Since the instability of the mutant crystals required data collection at cryogenic temperatures, it was first necessary to refine the wild-type structure against a cryogenic data set as a basis for comparison. The wild-type structure refined against 1.75 Å cryogenic data essentially is the same as the structure reported in 1987 (*4*). The overall rms difference in main chain backbone atoms is 0.2 Å between the room-temperature and cryogenic structures. The most notable changes are in the solvent structure. A total of 408 solvent molecules have been located in the cryogenic structure compared to 204 in the room-temperature structure. Three cryoprotectant solvent molecules, glycerol, also have been located.

Another notable feature in solvent structure is the definitive identification of the cation binding site (Figure 6). Previously (*4*), the cation location was based on the rather low temperature factor when this site was modeled as a water molecule and the fact that the site was surrounded by oxygen ligands. At that time, however, it was not possible to definitively assign this site as a cation since peaks in Fo-Fc difference maps were not large enough to distinguish between a low-temperature factor water, ammonium ion, or something larger. In contrast, the cryogenic structure shows extra positive Fo-Fc density at 6σ right on the water oxygen atom that has been modeled in the room-temperature structure. In addition, the temperature factor for the water refines to 2.0 Å^2, the minimum allowed by XPLOR. Clearly, something larger than water occupies this site. When modeled as a potassium ion, the cation temperature factor refines to 22 Å^2 indicating that potassium is a reasonable model. The ligands consist of four peptide carbonyl oxygen atoms and two water molecules arranged in octahedral geometry. The average ligand−cation distance of 2.73 Å agrees well with that expected of oxygen−K^+ distances and is much larger than the 2.4 Å distance expected for Na^+ or Ca^{2+} (*31*). It should be noted that the cation−ligand distances and interactions were not restrained during the refinement. One final reason for suspecting potassium is the functional connection between potassium and substrate binding since camphor binds more readily to the active site in the presence of potassium (*32*). Note that one of the ligands to the cation is the carbonyl group of Tyr96 and that the Tyr96 side chain hydroxyl group hydrogen-bonds with the substrate, camphor (Figure 6). The direct connection between K^+ ions, Tyr96, and substrate binding has been demonstrated using site-directed mutagenesis (*33*, *34*). As concluded earlier, it appears that the cation helps to stabilize Tyr96 in a conformation that favors the Tyr96−substrate hydrogen-bond (*4*).

Asp251Asn Structure. Figure 7 shows an initial Fo-Fc electron density map around the site of mutation. The map clearly indicates movement of Asn251, Lys178, Asp182, and Arg186. Changes are confined to this region of the structure. The overall root-mean-square difference in backbone atoms between the mutant and wild-type cryogenic structures is 0.17 Å. In the wild-type structure, Asp251 forms a set of hydrogen-bond/ionic interactions with Thr185, Arg186, and Lys178 (Figure 8). In the Asp251Asn mutant, these interactions are disrupted (Figure 8). The Asn251 and Lys178 side chains rotate toward the surface and are about 2 Å further

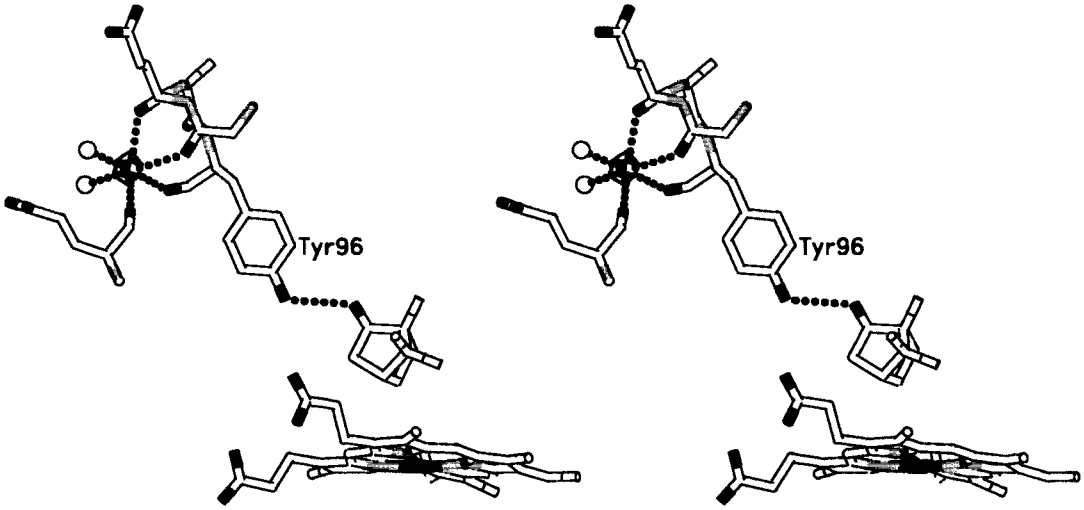

FIGURE 6: Stereo diagram showing the cation binding site in the wild-type cryogenic structure superimposed on the Fo-Fc omit electron density map contoured at 10σ. The two small spheres are water molecules coordinated to the cation and the remaining ligands are peptide carbonyl oxygen atoms.

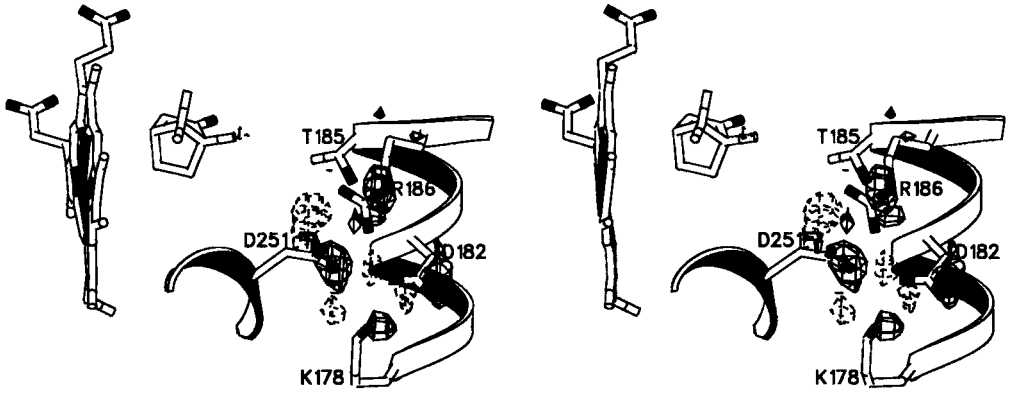

FIGURE 7: Stereo diagram of the initial 1.9 Å Fo-Fc electron density map contoured at +3.5σ superimposed on the wild-type structure. Phases were taken from the refined wild-type cryogenic structure and the amplitudes from the Asp251Asn mutant data set.

apart than in the wild-type structure and hence no longer form a hydrogen-bond. The hydrogen-bond with Thr185 also is lost. However, the new position of Asn251 allows a new hydrogen-bond to form with Asp182. The rupture of the 251−185 hydrogen-bond and rotation of the Asn251 side chain toward the surface provides a new opening to the active site pocket that is not present in the wild-type structure (Figure 9).

DISCUSSION

One of the primary goals in understanding the O_2 activation reaction in P450s is the identification of the chemical functionality that delivers a proton to the iron-linked dioxygen. Unlike other enzymes, there is no strategically positioned acid−base catalyst such as the His in peroxidases (*35*) that is an obvious choice as the catalytic residue. Instead, it has been necessary to postulate rather complicated proton delivery mechanisms for which only indirect evidence is available. The closest structural evidence to date on the identity of the proton delivery group is with P450eryF (*36*). In this structure, a water molecule is positioned only 3.8 Å from the iron and hence is in an ideal position to deliver a proton to the iron-linked dioxygen (*37*). P450cam, however, does not have a similarly positioned water visible in electron density maps, so it has been necessary to postulate the presence of a water in the oxy complex that serves as the proton donor.

Overall, P450cam appears to have several possible routes of proton delivery. An analogous path to that described above involves the highly conserved Glu366 and an array of highly ordered solvent molecules that connects this residue into the active site with an additional highly conserved alcohol functionality contributed by Thr252. This hydrogen-bonding network is very similar to the one observed in P450eryF, except P450eryF uses a water molecule in place of the P450cam Thr252 to directly interact with bound dioxygen. Based on the results of the molecular dynamics simulations, Harris and Loew (*38*) proposed this network to be the proton donor in P450eryF and, by inference, that in P450cam. However, whereas mutations of other active site residues thought to be involved in proton transfer resulted in drastic effects on activity, only a moderate decrease in the rate of NADH oxidation was observed in a reconstituted system with the mutant Glu366Gln in P450cam (*39*). This preliminary result, together with a lack of observed water connectivity from Glu366 to the solvent surface in P450cam, casts some doubt on the role of this residue in catalytic proton transfer.

Another water exit pathway was recently proposed (*40*) which extends from the propionate A side chain and Arg299 to the protein surface. This path could offer an attractive way of water molecule displacement from the active site upon substrate binding. Moreover, since this internal water

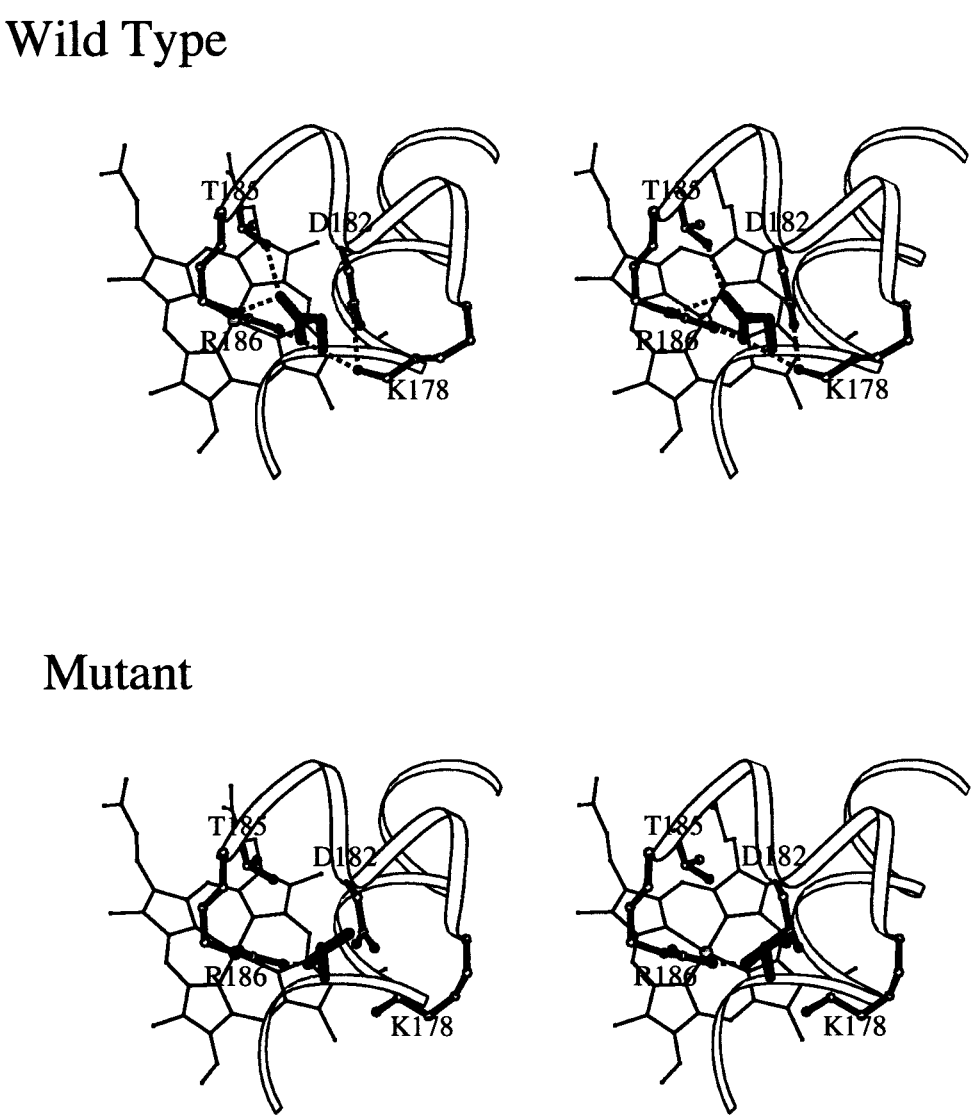

FIGURE 8: Stereo diagrams showing the wild-type and Asp251Asn mutant structures in the vicinity of the mutation site. Hydrogen-bonding interactions are shown as dotted lines.

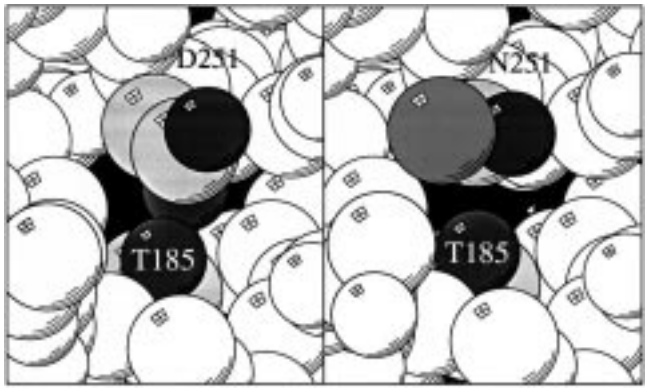

FIGURE 9: Space filled diagrams comparing the interaction between Asp251 and Thr185 in the wild-type and mutant structures. For residues 251 and 185, the side chain atoms are shaded in the following order (light to dark): carbon, nitrogen, oxygen. The surrounding atoms from other residues are all in white, while the heme is black. Note that the disruption of the Asp251−Thr185 hydrogen-bond in the mutant and subsequent rotation of Asn251 out and away from the active site leaves a slightly larger opening above the heme pocket.

cluster communicates with the bulk water, it could, in principle, also be responsible for proton delivery necessary for oxygen bond scission. The bi-directional role of this so-called aqueduct is, however, complicated by the position of the Arg299 side chain which needs to assume different rotamer conformations in order to allow communication between the active site and surface solvent molecules. Additional experiments involving mutagenesis and solvent isotope effects are needed to fully assess the possibility of proton transfer by this route.

The third proposed route of proton entry involves Asp251 (Figure 10). In this scheme Asp251 serves as a "carboxylate switch" that shuttles protons from the surface accessible catalytic triad (R186, K178, D182) to a bound water in the active site (*15*). Mutation of Asp251 to Asn disrupts this highly specific proton delivery mechanism, forcing the protein to find an alternative method for proton delivery. The large increase in KSIE in the mutant protein reported herein, together with the proton inventory analysis, indicates that a much larger number of protons are involved in the transition in the Asp251Asn mutant. This could be explained by additional solvent molecules, possibly five to seven, fulfilling the role of the Asp251 proton delivery machinery.

The mutant crystal structure is consistent with this view. The Asp251Asn mutant structure shows that the array of

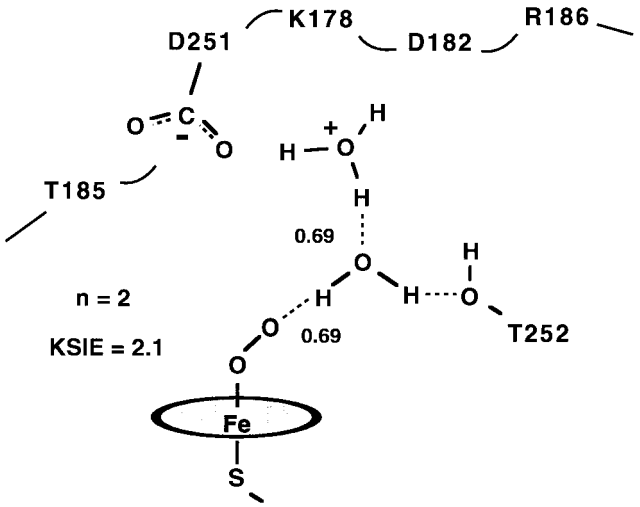

FIGURE 10: Proton delivery model for wild-type P450cam. Asp 251 serves as a "carboxylate switch" allowing communication between solvent accessible residues (Lys178, Asp182, and Arg186) and the catalytic water molecules in the active site. Calculated KSIE for two protons "in flight" with expected functional group fractionation factors of 0.69 (*18, 29*) yields overall isotope effect of 2.1, in good agreement with the experimentally measured value of 1.8 (*18*).

hydrogen-bond/ion pairs involving Asp251 is disrupted. Most importantly, the new Asn251 amide side chain no longer favors hydrogen-bonding with Thr185, but instead rotates out and away from the active site to form a new hydrogen-bond with Asp182. Asn251 still interacts with Arg186, but the Aps251-Lys178 interaction is lost. It is interesting to note that conversion of Lys178 to Gln does not have a large effect on activity (*14*). This glutamine could still hydrogen-bond with Asp251, but even if it does not, a disruption of the Asp251−Lys178 interaction should not alter the position of Asp251. Rather, it is the Thr185−Asp251 hydrogen-bond that may be the key in orienting Asp251 "in" toward the active site. This further suggests that the "in" orientation of Asp251 is important for acid−base catalysis. The "out" orientation in the mutant structure opens the active site which would make bulk solvent more accessible to the iron-linked dioxygen, thereby providing the alternate solvent-based proton delivery pathway indicated by the KSIE results.

An important result from this investigation is that it still is necessary to postulate the existence of new catalytic waters in the active site (Figure 10) and, possibly, conformational changes that enable Asp251 to participate in a protein−solvent hydrogen-bonding network that shuttles protons to the iron-linked dioxygen. Fortunately, there is some crystallographic evidence that supports such movement. Poulos and Howard (*41*) determined the structure of a series of inhibitors bound to P450cam. One of these, 2-phenylimidazole, binds with the phenyl moiety close to the heme and the imidazole group close to Asp251. A new water moves into the heme pocket that serves as a hydrogen-bonding bridge between Asp251 and the imidazole group. In addition, the entire I-helix, of which Asp251 is a part, slides closer to the inhibitor, and Thr185 rotates around such that its side chain hydroxyl function hydrogen-bonds with the new water. Overall, the motions and presence of a new water observed in the inhibitor−P450cam complex are similar to what is required by the mechanism shown in Figure 10. It also appears that water operating as the direct proton donor to the iron-linked dioxygen will be a general feature shared by all P450s (*37*). The specific pathway and set of residues employed may differ, however, and will depend on the size, shape, and electrostatic properties of the active site which, in turn, depends on substrate specificity requirements.

An alternative interpretation of the isotope effect data involves the participation of the reactant state in the observed KSIE (R. L. Schowen, personal communication). The corresponding model would include twice-reduced iron-ligated dioxygen with an estimated fractionation factor $\phi^{RS} \approx 0.43$. The overall isotope effect originating from the transition state would then increase, necessitating the participation of three protons "in flight". However, this interpretation does not rule out the proposed model in Figure 10 since a three proton model with $\phi^{TS} = 0.63$ and $\phi^{RS} = 0.43$ would result in total KSIE of 1.72. Furthermore, by the same analysis the number of protons involved in the substrate turnover catalyzed by Asp251Asn mutant is augmented to nine, suggesting that the mechanism of proton transfer is indeed different in these two proteins.

In conclusion, it appears that P450cam has evolved to maintain a highly specific proton delivery mechanism in order to avoid the unwanted production of hydrogen peroxide via nonspecific electron donation to dioxygen. The use of "carboxylate switches" as a means of specific proton delivery may not be unique to P450cam. Similar mechanisms have been suggested for proton pump proteins such as bacteriorhodoposin (*42*, *43*) and cytochrome oxidase (*44*).

ACKNOWLEDGMENT

We thank SSRL staff for their assistance in synchrotron data collection and Sharaeh Tajbakhsh and Amy Caygill for assistance in protein preparation. S.G.S. and M.V. also thank Dr. Richard Schowen and Dr. Mark McLean for insightful discussions and Ms. Aretta Weber for her editorial expertise.

REFERENCES

1. Yu, C.-A., and Gunsalus, I. C. (1974) *J. Biol. Chem. 249*, 94−101.
2. Haniu, M., Armes, L. G., Yasunobu, K. T., Shastry, B. A., and Gunsalus, I. C. (1982) *J. Biol. Chem. 257*, 12664−12671.
3. Koga, H., Rauchfuss, B., and Gunsalus, I. C. (1985) *Biochem. Biophys. Res. Commun. 30*, 412−417.
4. Poulos, T. L., Finzel, B. C., and Howard, A. J. (1987) *J. Mol. Biol. 195*, 687−700.
5. Poulos, T. L., Finzel, B. C., and Howard, A. J. (1986) *Biochemistry 25*, 5314−5322.
6. Ravichandran, K. G., Boddupalli, S. S., Hasemann, C. A., Peterson, J. A., and Deisenhofer, D. (1993) *Science 261*, 731−736.
7. Li, H., and Poulos, T. L. (1995) *Acta Crystallogr., Sect. D 51*, 21−32.
8. Li, H., and Poulos, T. L. (1997) *Nat. Struct. Biol. 4*, 140−146.
9. Raag, R., and Poulos, T. L. (1989) *Biochemistry 28*, 7586−7592.
10. Eble, K. S., and Dawson, J. H. (1984) *J. Biol. Chem. 259*, 14389−14393.
11. Imai, M., Shimada, H., Watanabe, Y., Matsushima-Hibiya, Y., Makino, R., Koga, H., Horiuchi, T., and Ishimura, Y. (1989) *Proc. Natl. Acad. Sci. U.S.A. 86*, 7823−7827.
12. Martinis, S. A., Atkins, W. M., Stayton, P. S., and Sligar, S. G. (1989) *J. Am. Chem. Soc. 111*, 9252−9253.
13. Raag, R., Martinis, S. A., Sligar, S. G., and Poulos, T. L. (1991) *Biochemistry 30*, 11420−11429.
14. Shimada, H., M. R., Imai, M., Horishi, T., and Ishimura Y. (1990) in *International Symposium on Oxygenases and Oxygen*

Activation (Yamamoto, S, N. M., and Ishimura, Y., Eds.) pp 133, Yamada Science Foundation,
15. Gerber, N. C., and Sligar, S. G. (1992) *J. Am. Chem. Soc. 114*, 8742−8743.
16. Gerber, N. C., and Sligar, S. G. (1994) *J. Biol. Chem. 269*, 4260−4266.
17. Benson, D. E., Suslick, K. S., and Sligar, S. G. (1997) *Biochemistry 36*, 5104−5107.
18. Aikens, J., and Sligar, S. G. (1994) *J. Am. Chem. Soc. 116*, 1143−1144.
19. Salomaa, P., Schaleger, L. L., and Long, F. A. (1964) *J. Am. Chem. Soc. 86*, 1−7.
20. Poulos, T. L. (1996) *Methods Enzymol. 272*, 358−368.
21. Kabsch, W. (1993) *J. Appl. Crystallogr. 26*, 795−800.
22. Brunger, A. T. (1992) *X-PLOR: A system for crystallography and NMR. Version 3.1*, Yale University Press, New Haven, CT.
23. 4, C. C. P. (1994) *Acta Crystallogr., Sect. D 50*, 760−763.
24. Otwinowski, Z. (1992) *DENZO: An oscillation data processing program for macromolecular crystallography*, Yale University Press, New Haven, CT.
25. Jones, T. A. (1985) *Methods Enzymol. 115*, 157−171.
26. Navaza, J. (1994) *Acta Crystallogr., Sect. A 50*, 157−163.
27. Mueller, E. J., Loida, P. J., and Sligar, S. G. (1995) in *Cytochrome P450. Structure, Mechanism, and Biochemistry* (Ortiz de Montellano, P. R., Ed.) pp 83−124, Plenum Press, New York.
28. Quinn, D. M., and Sutton, L. D. (1991) in *Enzyme Mechanism from Isotope Effects* (Cook, P. F., Ed.) pp 73−126, CRC Press, Boca Raton, FL.
29. Schowen, R. L. (1977) in *Isotope Effects on Enzyme-Catalyzed Reactions* (Cleland, W. W., O'Leary, M. H., and Northrop, D. B., Eds.) pp 64−99, University Park Press, Baltimore.
30. Shimada, H., Sligar, S. G., Yeom, H., and Ishimura, Y. (1997) in *Oxygenases and Model Systems* (Funabiki, T., Ed.) pp 195−221, Kluwer Academic Publishers, Dordrecht, The Netherlands.
31. Glusker, J. P. (1991) *Adv. Protein Chem. 42*, 1−76.
32. Peterson, J. (1971) *Arch. Biochem. Biophys. 144*, 678−693.
33. Atkins, W. M., and Sligar S. G. (1988) *J. Biol. Chem. 263*, 18842−18849.
34. Di Primo, C., Hui Bon Hoa, G., Douzou, P., and Sligar, S. G. (1990) *J. Biol. Chem. 265*, 5361−5363.
35. Poulos, T. L., and Finzel, B. (1984) in *Peptide and Protein Reviews* (Heran, M. T. W., Ed.) pp 115−171, Marcel Dekker, New York.
36. Cupp-Vickery, J. R., and Poulos, T. L. (1995) *Nat. Struct. Biol. 2*, 144−153.
37. Cupp-Vickery, J. R., Han, O., Hutchinson, R., and Poulos, T. L. (1996) *Nat. Struct. Biol. 3*, 632−637.
38. Harris, D., and Loew, G. (1996) *J. Am. Chem. Soc. 18*, 6377−6387.
39. Vidakovic, M., and Sligar, S. G. (manuscript in preparation).
40. Oprea, T. I., Hummer, G., and Garcia, A. E. (1997) *Proc. Natl. Acad. Sci. U.S.A. 94*, 2133−2138.
41. Poulos, T. L., and Howard, A. J. (1988) *Biochemistry 26*, 8165−8174.
42. Checover, S., Nachliel, E., Dencher, N. A., and Gutman, M. (1997) *Biochemistry 36*, 13919−13928.
43. Pebay-Peyroula, E., Rummel, G., Rosenbusch, J. P., and Landau, E. M. (1997) *Science 277*, 1676−1681.
44. Mitchell, D. M., Fretter, J. R., Mills, D. A., Adelroth, P., Pressler, M. A., Kim, Y., Aasa, R., Brzezinski., P., Malmstrom, B. G., Alben, J. O., Babcock, G. T., Ferguson-Miller, S., and Gennis, R. B. (1996) *Biochemistry 35*, 13089−13093.

BI980189F